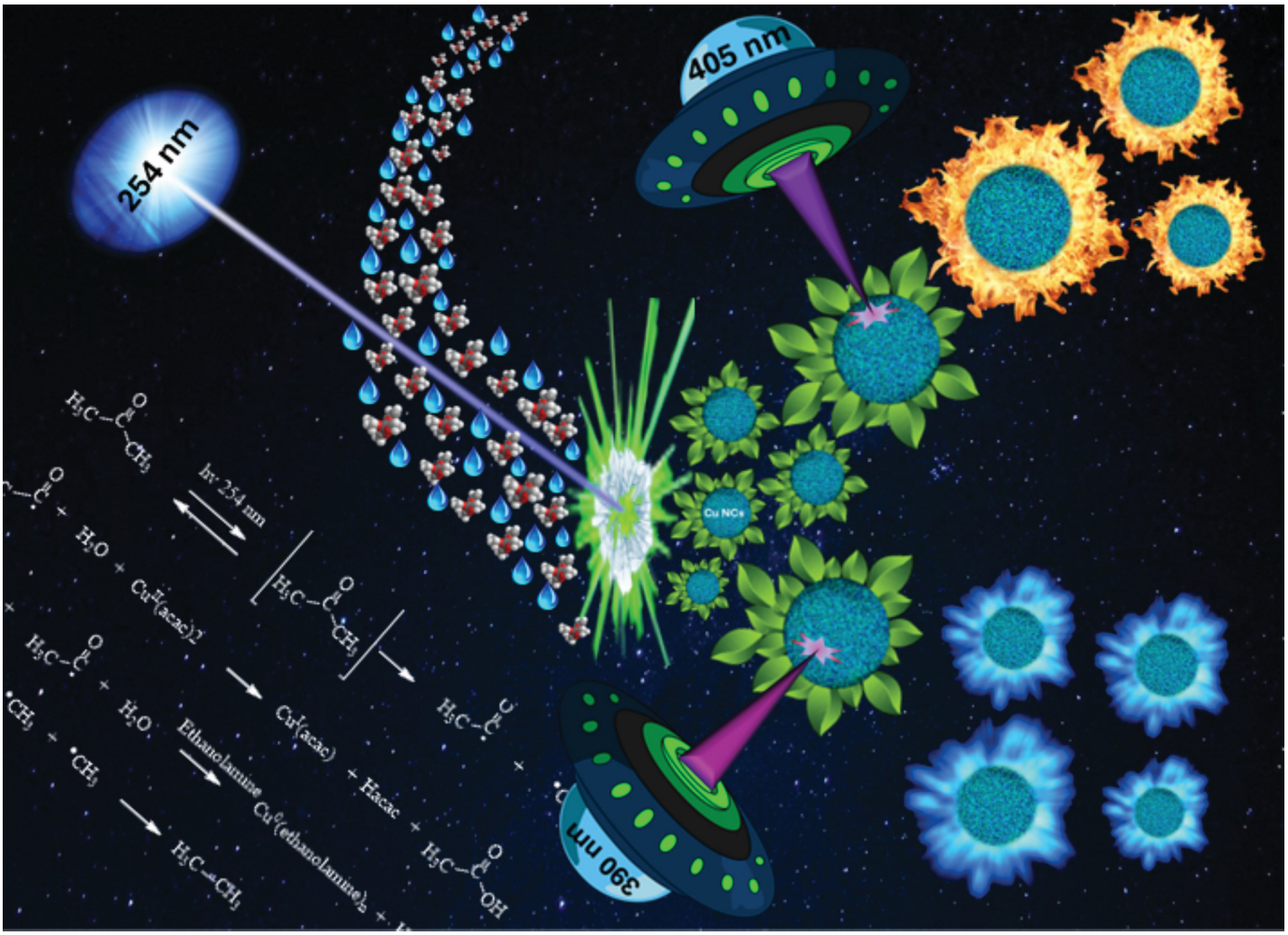

Showcasing research from Professor Antonino Gulino's laboratory, School of Chemistry, University of Catania, Italy, Catania.

Photochemical eco-friendly synthesis of photothermal and emissive copper nanoclusters in water: towards sustainable nanomaterials

A green photochemical synthesis of stable and robust Cu nanoclusters from an aqueous solution of copper acetylacetonate. The obtained nanoclusters irradiated at 405 nm showed excellent photothermal properties while excited at 390 nm displayed excellent luminescent properties suitable for future applications in many technological fields.

As featured in:

See Angelo Ferlazzo, Salvatore Petralia, Andrea Caneschi, Antonino Gulino *et al.*, *Mater. Adv.*, 2024, **5**, 8034.

ROYAL SOCIETY OF CHEMISTRY

rsc.li/materials-advances

Registered charity number: 207890

Materials Advances

ROYAL SOCIETY OF CHEMISTRY

PAPER

View Article Online
View Journal | View Issue

Cite this: *Mater. Adv.*, 2024, 5, 8034

Photochemical eco-friendly synthesis of photothermal and emissive copper nanoclusters in water: towards sustainable nanomaterials†

Angelo Ferlazzo,*[a] Stefano Bonforte,[a] Federica Florio,[a] Salvatore Petralia,*[b] Lorenzo Sorace,[c] Beatrice Muzzi,[d] Andrea Caneschi*[e] and Antonino Gulino*[a]

Received 17th April 2024,
Accepted 5th August 2024

DOI: 10.1039/d4ma00401a

rsc.li/materials-advances

The pursuit of sustainable and environmentally benign approaches to nanomaterial synthesis has gained significant momentum in recent years. Copper is rather cheap and more abundant than gold or silver and small copper nanoclusters (~1 nm) show unique characteristics which makes them extremely attractive for technological applications. Among these endeavours, the development of eco-friendly methods for the synthesis of copper nanoclusters (Cu NCs) in aqueous environments has emerged as a promising avenue. This shift towards green syntheses not only addresses the growing concerns regarding the environmental impact of conventional synthetic routes but also offers a platform for producing Cu NCs with tailored properties for diverse applications. In the present study, we report on a green photochemical approach to synthesising water-dispersible copper nanoclusters capped with monoethanolamine to confine their size. The obtained material was characterized by a large palette of techniques, including UV-vis spectroscopy, fluorescence spectroscopy, electron paramagnetic resonance, X-ray photoelectron spectroscopy, Z-potential analysis, cyclic voltammetry, field-dependent magnetization, scanning transmission electron microscopy and dynamic light scattering. The results unequivocally demonstrate that the Cu NCs are temporally and thermally stable for months, therefore promising for technological uses.

Introduction

In the last few decades, research into nanomaterials has made countless threads. For example, many studies have focused on the fabrication of carbon and semiconducting quantum dots, ultra-small noble metal particles, and nanosized metal oxides for catalysis, molecular recognition *etc.*[1] To improve the chemical stability and uniformity at the atomic level, enhance their electrical, magnetic, and optical properties and to decrease their possible toxicity, it is essential to investigate new synthetic strategies.[2]

In addition, when the size of these nanomaterials approaches the Fermi wavelength of an electron, unique size-dependent properties have been observed. For instance, gold, silver or copper nanoparticles composed of tens or a few hundred atoms, referred to as nanoclusters (NCs), show optical and catalytic properties as well as other features, much different from those observed for bulk metals.[3–5]

Noble metal NCs are currently synthesized by exploiting different protective/capping ligands (*e.g.* polymers, organic molecules, *etc.*) that also help to confine their size growth.[6,7] These ligands interact with the cluster surface atoms in such a way to embed the given cluster to saturate the surface atom coordination sites, thus enhancing the physicochemical stability of NCs.

In this field many studies have been devoted to the fabrication of gold and silver NCs while copper NCs have attracted much lower attention because of their tendency to oxidation; only recently research showed renewed interest toward these systems, finalized to improve their stability and properties.[8,9] As a few examples, it has been shown that the excellent fluorescence properties of some Cu NCs can be optimized by using different experimental conditions during their synthesis (solvent, pH, temperature, capping ligands *etc.*).[8] Similarly, Ag NCs show fluorescence intensity inversely

[a] *Department of Chemical Sciences and INSTM Research Unit, University of Catania, Viale Andrea Doria 6, 95125 Catania, Italy. E-mail: antonino.gulino@unict.it*
[b] *Department of Drug and Health Science, University of Catania, Via Santa Sofia 64, 95125 Catania, Italy and Institute of Biomolecular Chemistry, CNR, Via Paolo Gaifami 18, 95126, Catania, Italy. E-mail: salvatore.petralia@unict.it*
[c] *Department of Chemistry "U. Schiff" and INSTM Research Unit, University of Florence, 50019 Sesto Fiorentino (FI), Italy*
[d] *CNR-ICCOM – Istituto di Chimica dei Composti Organometallici, 50019 Sesto Fiorentino (FI), Italy*
[e] *Department of Industrial Engineering (DIEF) and INSTM Research Unit, University of Florence, 50139 Florence, Italy*

† Electronic supplementary information (ESI) available: Fig. S1. Luminescence emission stability of the final Cu NCs; Fig. S2. CV of Cu NCs recorded 5 months after the synthesis. Fig. S3. UV-vis spectrum of the final Cu NC solution eight months after the synthesis. Fig. S4. Photothermal conversion efficiency. See DOI: https://doi.org/10.1039/d4ma00401a

proportional to their size,[10–12] and also the emission of Au NC aggregates has been ascribed to ligand-to-metal charge transfer or ligand-to-metal–metal charge transfer from the sulphur of the thiolate ligands to the Au atoms and consequent radiative relaxation *via* a metal-centred triplet state.[13]

In this general context, some approaches for the synthesis of stable copper NCs have been reported such as electrochemical, milling, etching, reducing (mainly with ascorbic acid), template-assisted (proteins, enzymes, DNA and polymers as templates) and ligand-capped methods.[14] Among these, the synthesis of Cu NCs using reducing agents is certainly the most widely used, whereas green syntheses (absence of organic solvents) have been little investigated.

Among the various synthetic approaches, the photochemical method offers the advantage of being reagent-free while allowing easy process control, particularly as regards the exposure time and the intensity of the exciting light. Moreover, the metal precursor's optical properties can be used to tune the size, morphology, and amount of the nanostructures.

There are a few examples in the literature of photochemical reactions to produce Cu NCs using ethanol as a solvent.[15–17] To our knowledge, only one example of the synthesis of Cu NCs by photoreduction using copper chloride as a precursor in water has been reported by Gui *et al.*, who precipitated Cu NCs with propanol from a buffer solution and then redissolved them in water.[18] The utilization of water as a solvent presents an attractive alternative to traditional chemical routes for the synthesis of Cu NCs. This approach not only mitigates the use of hazardous reagents and organic solvents but also facilitates the integration of Cu NCs into aqueous-based systems, expanding their applicability in biomedical, environmental, and catalytic applications.

Therefore, in our present study, we report on the green photochemical synthesis of Cu NCs, consisting of the UV light (254 nm) irradiation of a copper(II) acetylacetonate ($Cu^{II}(acac)_2$) precursor in the presence of a photosensitizer (acetone) and monoethanolamine (MEA) as a capping agent in a deaerated aqueous solution, and we delve into the precise control over size, morphology, and surface properties. By focusing on the eco-friendly synthesis of Cu NCs in water, this paper aims to underscore the importance of sustainable approaches in nanomaterial synthesis while highlighting the potential of Cu NCs as environmentally friendly alternatives for diverse technological applications. The obtained Cu NCs in water were found to be stable for months, and this behaviour is due to the monoethanolamine capping layer which, on the one hand, limits the growth of the nanoclusters by confining them to a few nanometres, and on the other hand, almost seals the obtained nanoclusters, giving them high stability. The Cu NCs exhibited an excellent photothermal conversion efficiency upon blue-light exposure (405 nm).[19–22]

Experimental

Synthesis of copper nanoclusters

High-grade copper(II) acetylacetonate (hereafter $Cu(acac)_2$) 99.9%, monoethanolamine (MEA), water and acetone for spectrophotometric use were purchased from Sigma Aldrich. We prepared a stock 1.649×10^{-4} M water solution of $Cu(acac)_2$ by adding 4.317 mg of copper(II) acetylacetonate (MM = 261.76 g mol^{-1}; 1.6492×10^{-5} mol) in 100 mL of distilled water while stirring for 2 hours (solubility in water of $Cu(acac)_2$ = 0.2 g L^{-1}). The MX5 Microbalance Metter Toledo© (resolution 0.8–0.9 μg) was used for weighing chemicals. It is necessary to stabilize the as-obtained Cu NCs with an appropriate capping agent and, after some experiments, we have chosen to add to the starting copper solution 60 μL of monoethanolamine (δ = 1.02 g mL^{-1}, MM = 61.084 g mol^{-1}, 1.002×10^{-3} mol) diluted in 6 mL of water, and 7 mL of pure acetone (photosensitizer) before irradiation.[23] Therefore, the resulting Cu(II) and MEA concentrations (113 mL total volume) are 1.459×10^{-4} and 8.87×10^{-3} M, respectively. This last solution was sealed in a quartz reaction tube and irradiated in a reactor at 254 nm with four Helios Quartz© lamps (UVC power intensity 4 W cm^{-1} per each), under a constant argon flux (100 sccm min^{-1}) for 180 minutes and left under argon flux for additional 50 minutes in the dark to remove gaseous reaction products. The reactor is equipped with a fan to prevent overheating. The obtained yellow solution was concentrated to 6 mL using a rotavapor. The concentrate was centrifuged at 13 000 rpm for 30 minutes, filtered through a 0.2 μm filter and lyophilised ($T = -20$ °C) thus obtaining an oil. Dynamic light scattering measurements evidenced that the dispersion of Cu NCs in water possesses a mean hydrodynamic diameter (volume %) of around 60.9 ± 6.7 nm at 25 °C, with a Z-potential value of −10.2 ± 2.5 mV. The hydrodynamic radius value obtained by dynamic light scattering (DLS) analysis depends on the water capping layer that covers the Cu NCs (already capped with monoethanolamine), thus increasing the overall volume. In fact, the DLS theory states that the electric dipole layer of both the capping layer and the solvent adhering to the surface of the particles influences their movement in the medium. Thus, the hydrodynamic diameter gives information about the inorganic core along with any coating materials and solvent layers attached to the particle. For example, it has been reported that the diameter of some Fe_3O_4 particles was found to be 25 nm from TEM, whereas their average hydrodynamic size was 164 nm from DLS. Therefore, the size of Cu NCs remains the same as that obtained with TEM measurements (*vide infra*).[24]

Characterization methods

X-ray photoelectron measurements. X-ray photoelectron spectra (XPS) were recorded at a 45° take-off angle relative to the surface sample holder, using a PHI 5000 Versa Probe II system (ULVAC-PHI, INC., base pressure of the main chamber 1×10^{-8} Pa).[24,25] The samples were excited with the monochromatized Al Kα X-ray radiation with a pass energy of 5.85 eV. The instrumental energy resolution was ≤0.5 eV. The XPS peak intensities were obtained after Shirley's background removal. Spectra calibration was achieved by fixing the Ag $3d_{5/2}$ peak of a clean sample at 368.3 eV.[26,27] The atomic concentration analysis was performed by considering the relevant atomic sensitivity factors. The fitting of some XP spectra was carried out, using the XPSPEAK4.1 software, by fitting the spectral profiles with

symmetrical Gaussian envelopes, after subtracting the background. This process involves data refinement, based on the method of the least squares fitting, carried out until there is the highest possible correlation between the experimental spectrum and the theoretical profile. The residual or agreement factor R, defined by $R = [\Sigma (F_{obs} - F_{calc})^2 / \Sigma (F_{obs})^2]^{1/2}$, after minimization of the function $\Sigma (F_{obs} - F_{calc})^2$, converged to the value of 0.03.

UV-vis spectra. UV-vis spectra were obtained using a UV-vis V-650 Jasco spectrometer with a resolution of 0.1 nm at room temperature. Measurements were performed using a 1 cm quartz cuvette. The UV-vis spectrum of the final water solution, before lyophilization, was measured using a 0.1 cm quartz cuvette.

Photoluminescence spectra. Photoluminescence (PL) spectra were recorded using a Jasco FP-8350ST spectrofluorometer (Xe lamp, JASCO Europe Srl, Cremella, Italy) with a λ_{exc} of 390 nm[28] and a resolution of 1 nm at room temperature. The emission was recorded at 90° to the direction of the exciting light with a slit width of 5 : 5 nm. The photoluminescence quantum yield (ϕ_{PL}) of the dispersion of Cu NCs in water (n = 1.33) was obtained using a solution of quinine sulphate (n = 1.36) as a standard (ϕ_{PL} = 0.55).

DLS analysis. Particle size and surface charge were investigated using a ZetaSizer NanoZS90 (Malvern Instrument, Malvern, UK) equipped with a 633 nm laser (90° scattering angle and a temperature of 25 °C).

Photothermal analysis. The photothermal properties of Cu NCs were investigated by irradiating 100 μL of the Cu NCs in a quartz tube with a CW laser emitting at 405 nm, using various laser powers for various minutes. We used a FLIR infrared thermal imaging camera to measure the temperature of the solution every 10 s, during the heating and cooling process. The photothermal conversion yield (η%) was calculated using Roper's equation as described in the ESI† section.

Electrochemical measurements. Cyclovoltammetry measurements (CV) were performed using a DropSens μStat 400 potentiostat with Dropview 8400 software, in the standard configuration applying a potential scan from −0.9 to + 1.0 V with a scan rate of 50 mV s^{-1} using a cell containing 1 M KCl solution. It was chosen to start from negative potentials to highlight the presence of the oxidation peak from Cu^0 to Cu^{2+}. Both working and counter electrodes were screen printed carbon electrodes (SPCEs), while the reference electrode was a screen printed silver electrode (ceramic substrates 35 mm long and 4.0 mm in diameter covered with carbon or silver, Methrom DropSens). These electrodes were modified with a water solution of Cu NCs (Cu/SPCE) or $Cu(acac)_2$ (Cu^{2+}/SPCE) by depositing 10 μL of each solution (1.649×10^{-4} M water solution of $Cu(acac)_2$ or that obtained after its photochemical reduction) on the surface of the carbon working electrode using a drop casting technique.[29] The sensors thus manufactured were left to dry for 24 hours in air.

EPR spectroscopy and magnetic properties. X-band CW-EPR spectra of all samples were recorded using a Bruker Elexsys E500 spectrometer equipped with an SHQ cavity ($\nu \cong 9.40$ GHz with cryostat). Low-temperature measurements were obtained using an Oxford Instruments ESR900 continuous flow helium cryostat and the temperature was controlled using an Oxford Instrument ITC503. The sample dissolved in water was measured at 40 K after pre-freezing in liquid N_2. The same sample used for SQUID measurements was used to measure the EPR spectrum of the Cu NCs in oil form. Spectral simulations were performed using EasySpin.[30]

Magnetic characterization. Field (0–5 T) dependence of the magnetic moment of the obtained material has been measured at 5 K by using an MPMS SQUID magnetometer (quantum design) by wrapping in Teflon (8.66 mg) 2.55 mg of the obtained oil. Raw data were corrected for the diamagnetic Teflon contribution ($\chi_d = -3.7 \times 10^{-7}$ emu g^{-1}) and were converted to molar ones by assuming that the sample was exclusively composed of copper (*i.e.* data in emu g^{-1} were converted to emu mol^{-1} by multiplying the molar weight of copper (63.54 g mol^{-1})).

Scanning transmission electron microscopy (STEM). The STEM measurements were carried out using a TALOS F200X G2 microscope (Thermo-Fisher Scientific) equipped with a high-brightness field emission gun (X-FEG, 80–200 keV) operating in TEM and STEM mode, and with 4 in-column SDD Super-X detectors for energy dispersive X-ray spectroscopy (EDXS).

Results and discussion

Copper nanoclusters can be produced by photochemical approaches, involving the reduction of Cu ions in the presence of stabilizing agents under UV light. This procedure often leads to the formation of very small-sized and well-dispersed nanoclusters with unique properties. For this purpose, initially, we performed some preliminary tests to shed light on the behaviour of the photochemical reduction of the Cu(II) ion from $Cu(acac)_2$ in water using the UV-vis technique. The UV-vis spectrum of a 5.4966×10^{-5} M $Cu(acac)_2$ water solution (obtained by dilution of the initial stock solution) shows two bands at 238.5 nm (ε = 9200 M^{-1} cm^{-1}) and 292.6 nm (ε = 15 860 M^{-1} cm^{-1}) due to a ligand-to-metal charge transfer (LMCT) and to a π–π* (HOMO → LUMO) transition of the ligand, respectively (Fig. 1).[15] No other absorption bands were observed under these conditions since the d–d transition of the Cu(II) ion has an ε value ∼10 M^{-1} cm^{-1}. The UV-vis spectrum of the $Cu(acac)_2(MEA)_2$ complex, where the NH_2– group of the MEA capping agent saturates the two free axial positions of the Cu ion, shows a unique band envelope with a main absorption that is shifted from 292.6 to 283.4 nm, due to the reinforced ligand field.[31] Then, irradiation at 254 nm of the above solution (Fig. 1) caused a profound spectral change with a spectrum now dominated by a new band at 265.2 nm and two shoulders at ∼315 and 380 nm. Previously reported data on similar Cu NCs indicated the appearance of bands at almost identical positions; the 265.2 nm absorbance has been attributed to an intraligand nN → π* transition (at 260–275 nm for Cu NCs stabilized with glutathione),[32] the one at 315 nm to self-assembled Cu NCs (at the identical 315 nm position for Cu NCs stabilized with 4,6-dimethyl-2-mercaptopyrimidine)[33] and that at 380 nm to an enhanced interaction between Cu atoms and the electron-rich nitrogen atoms of MEA (reported at the

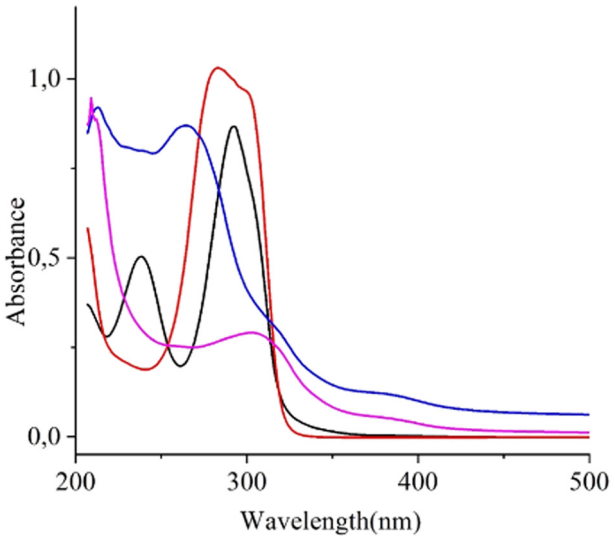

Fig. 1 UV-vis spectra of: 5.5×10^{-5} M $Cu(acac)_2$ water solution (black line); 5.5×10^{-5} M $Cu(acac)_2$ and 2.96×10^{-3} M monoethanolamine capping agent water solution (red line); 5.5×10^{-5} M $Cu(acac)_2$ and 2.96×10^{-3} M monoethanolamine capping agent water solution after 180 min irradiation at 254 nm followed by 50 min dwell of the resulting solution in the dark during continuous argon flux (see experimental details) (blue line); final solution after 24 h from the end of the irradiation and after a volume reduction to 6 mL, measured using a 0.1 cm quartz cuvette (pink line).

identical 380 nm position for Cu NCs stabilized with citrate anions).[34] After 24 h, the UV-vis spectrum is dominated by the 315 nm band, which undergoes a blue shift to 303.9 nm, while the shoulder at 380 nm remains. The presence of this shoulder at 380 nm and the absence of any plasmonic peak suggest the formation of small nanoclusters.

Fig. 2 shows the emission spectra of the 5.5×10^{-5} M $Cu(acac)_2$ water solution where the intensity was multiplied by 100 since this starting solution shows almost no emission. In contrast, the final Cu NCs solution, after 24 h from the end of irradiation, and after a volume reduction from 100 to 6 mL (*vide supra*), under the same excitation wavelength, shows an intense emission band at 489.9 nm with a full width at half-maximum (fwhm) of 100 nm and a high energy shoulder at ~460 nm. The increase in the emission after 24 h has been previously reported in this type of system and is a consequence of Cu NCs self-assembly, due to the coordination of Cu NCs with the capping agent that induces LMCT and/or LMMCT charge transfer.[35,36] The results of the emission experiments reported here are almost identical to those reported for the above-mentioned Cu NCs assemblies that exhibit a strong emission peak centred at 490 nm with an fwhm of 86 nm.[35] No major differences were observed in the emission spectrum as the excitation wavelength changed in the range of 330–410 nm. The photoluminescence quantum yield (ϕ_{PL}) of Cu NCs in water was calculated to be 0.12.

Furthermore, the stability of the emission properties of these Cu NCs was confirmed 7, 20, 26 and 32 days after the end of the reaction (Fig. S1, ESI†).

To resume, both UV-vis and emission measurements confirm the formation of small Cu nanoclusters.[8] Therefore, it

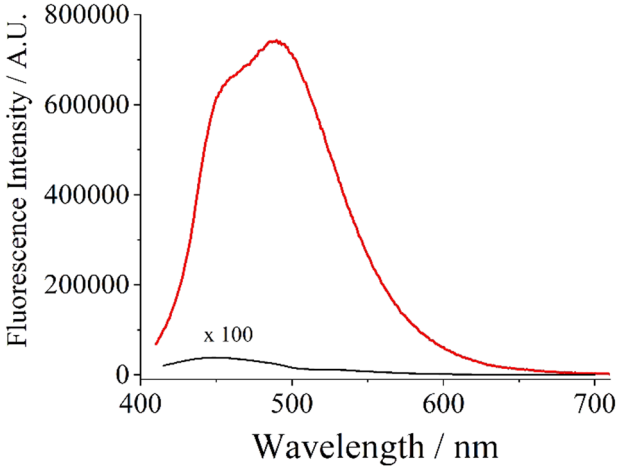

Fig. 2 Emission spectra, λ_{exc} = 390 nm, of 5.4966×10^{-5} M $Cu(acac)_2$ water solution (black line where the intensity was multiplied by 100) and final Cu NCs solution after 24 h from the end of the irradiation and after a volume reduction to 6 mL (red line).

emerged that the emission increases upon the increase of the Cu–Cu inter- and intra-NCs interactions,[37] and upon the restriction of the periodic motion (vibration and rotation) of the capping molecules that hampers the nonradiative relaxation of excited states.[38–41]

Concerning the possible reaction pathway (Scheme 1), irradiation of the photosensitizer (acetone) at 254 nm induces a $n \rightarrow \pi^*$ (S_0 to T_1) transition whose de-excitation produces both $CH_3CO^\bullet$ and $^\bullet CH_3$ reactive species. Interaction of the $CH_3CO^\bullet$ radical with $Cu^{II}(acac)_2$ in water results in the formation of $Cu^{I}(acac)$, acetylacetone (Hacac) and acetic acid. $Cu^{I}(acac)$ further reacts with another $CH_3CO^\bullet$ radical and another H_2O molecule to give Cu^0, Hacac and, again, acetic acid. The Cu^0 metal atoms in the presence of ethanolamine agent form small Cu^0 clusters capped by ethanolamine molecules that hamper the cluster size increase, thus avoiding some aggregation. The two $^\bullet CH_3$ species produce ethane. In tune with our supposed mechanism, we experimentally observed that the final solution had been acidic because of the formation of acetic acid.[19,42]

To confirm the formation of small Cu NCs, morphological and chemical composition analysis, was performed. STEM-HAADF images (Fig. 3) displayed small spherical polydisperse nanocrystals, with a narrow range size from 2.5 to 5 nm,

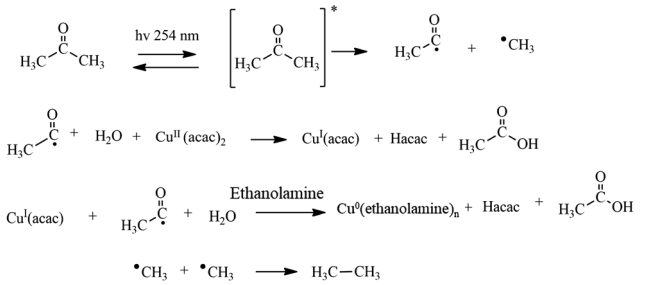

Scheme 1 Synthesized copper nanoclusters (Cu NCs) using a photochemical pathway.

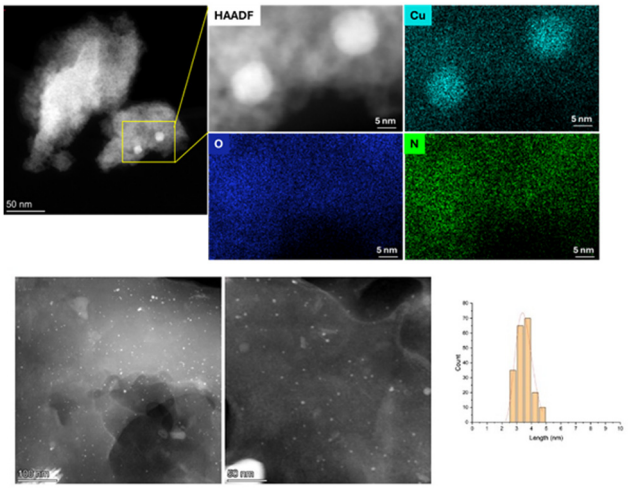

Fig. 3 (top) STEM-HAADF image of Cu NCs capped with ethanolamine and STEM-EDXS elements distribution maps; (bottom) TEM images with different magnifications also show the particle size distribution centred at 3.5 nm.

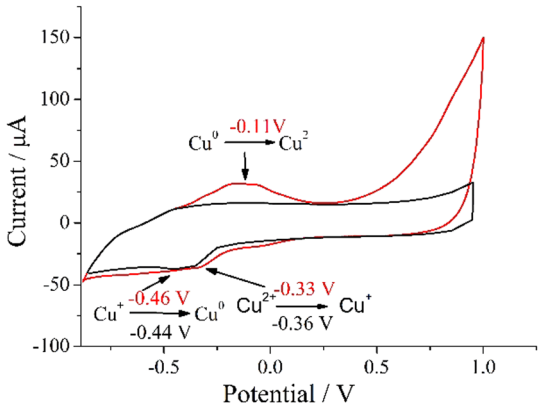

Fig. 4 CV of 5.4966×10^{-5} M $Cu(acac)_2$ water solution (black line and digits) and final Cu NCs solution after 24 h from the end of the irradiation and after a volume reduction to 6 mL (red line and digits).

dispersed in aggregates of ethanolamine. STEM-EDXS elemental mapping distribution, instead, confirmed the composition of the Cu NCs, and highlighted the retaining of Cu(II) ions complexed with ethanolamine, even after the reduction step (Fig. 3). Interestingly, only O of ethanolamine was observed, suggesting that no oxidation of the Cu NCs occurred.

Fig. 4 shows CV measurements for the starting $Cu(acac)_2$ and Cu NCs species. The surface area of Cu/SPCE is larger than that of Cu^{2+}/SPCE due to the presence of copper nanoparticles, and this fact results in a larger current range of the related CV curve.[43] The anodic oxidation peak ($Cu^0 \rightarrow Cu^{2+}$) is at −0.11 V. This value is consistent with that previously reported (−0.09 V) for a closed system measured with a similar electrode[42] and confirms the presence of Cu^0. In the cathodic phase, there is evidence of the Cu^{2+} to Cu^+ reduction, consistent with the peak at −0.33 V, followed by the $Cu^+ \rightarrow Cu^0$ reduction at −0.46 V. Both these values are in close agreement with those reported (−0.37 and −0.52 V) for a similar system.[44] The CV data indicate an anodic oxidation peak (I_{pa}) of 32.06 μA and a cathodic reduction peak (I_{pc}) of 34.95 μA. These two values are consistent with a completely reversible redox reaction; the small current difference of 2.89 μA between I_{pa} and I_{pc} can be attributed to the presence of a small amount of Cu^{2+}, less than 9% to the overall copper content in the measured representative Cu NC sample, also in agreement with magnetic measurements (*vide infra*). Five months after the synthesis, we repeated the CV measurements for the Cu NCs and obtained almost identical results thus demonstrating the long-term stability of the present Cu NCs (Fig. S2, ESI†). In addition, eight months after the synthesis, we recorded again the UV-vis spectrum of the final Cu NCs solution (Fig. S3, ESI†). The band at 303.9 nm remains unaltered, and this observation further confirms the excellent stability of these Cu NCs.

The successful synthesis of copper nanoclusters was further confirmed by studying their electronic structure using X-ray photoelectron spectroscopy (XPS), which provides information on the oxidation states and the chemical environment of the studied elements, and allows estimation of the surface elemental composition, once the relevant atomic sensitivity factors have been considered.[45,46] The two peaks at 932.4 and 952.4 eV observed in the Cu 2p binding energy region of the high-resolution XPS of the representative Cu NCs (Fig. 5A) are readily attributed to the Cu $2p_{3/2}$ and $2p_{1/2}$ spin–orbit pair and are strongly indicative of the presence of Cu^0 states.[47,48] Indeed, the presence of relevant Cu^{2+} species would result in an XPS spectrum which, apart from the two Cu 2p main spin–orbit couple, should show two additional Cu 2p peaks at ∼2 eV higher binding energy and intense satellite features centred at ∼942 and ∼962 eV. These additional peaks and satellites seem to be absent in the present spectrum or hidden under the noisy background, since the very low content of remaining Cu^{2+} species as detected by CV measurements (less than 9% of the overall copper content). In addition, by considering the reduction potentials of the different copper species in water solution ($Cu^{2+} + e \rightarrow Cu^+$ $E_0 = 0.15$ V; $Cu^+ + e \rightarrow Cu^0$ $E_0 = 0.52$ V; $Cu^{2+} + 2e \rightarrow Cu^0$ $E_0 = 0.34$ V), no stable Cu^+ species is expected in aqueous solution since any oxidant strong enough to convert Cu to Cu^+ would also convert Cu^+ to Cu^{2+} and Cu^+ ions are unstable toward disproportionation reaction: $2Cu^+ \rightarrow Cu^{2+} + Cu$ $E_0 = 0.37$ V, $K = 10^6$. Therefore, in an aqueous solution, only low equilibrium concentrations of Cu(I) can exist and XPS confirms that our synthetic procedure was effective in obtaining Cu^0 species in water solution. Fig. 5B shows the high-resolution XPS of the representative Cu nanoclusters in the N 1s binding energy region. The unique and rather symmetrical peak at 400.2 eV is due to the nitrogen of the monoethanolamine capping layer that stabilises the Cu nanoclusters.[49,50] Fig. 5C shows the XPS of the representative Cu nanoclusters in the C 1s binding energy region. A careful deconvolution of the experimental spectral profile required three Gaussians at 285.7, 286.9 and 288.7 eV due to the Cu–NH_2–C, –CH_2–OH and some –COO– functionalities (due to some acetic acid residues, see Scheme 1), respectively.[25,26] Fig. 5D shows the high-resolution XPS of the representative Cu nanoclusters in the O 1s binding energy region. The component at 532.0 eV is

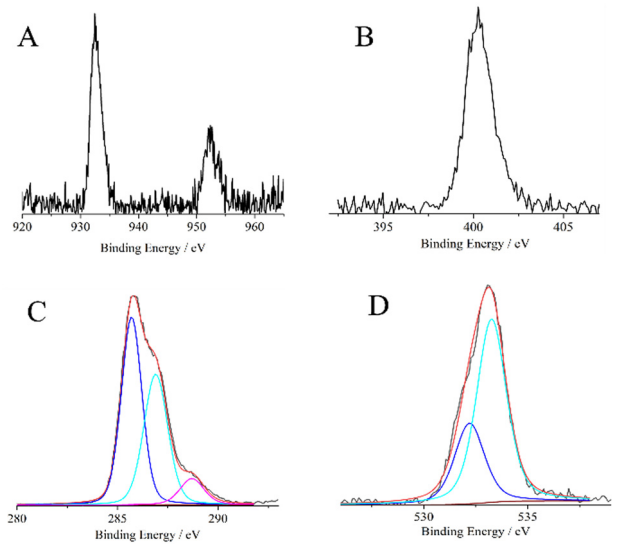

Fig. 5 Al-Kα excited XPS of the Cu nanoclusters in the Cu 2p (A) and N 1s (B) binding energy regions. Al-Kα excited XPS of the Cu nanoclusters in the C 1s (C) binding energy region: the blue, cyan and magenta Gaussians refer to the 285.7, 286.9 and 288.7 eV components, respectively. Al-Kα excited XPS of the Cu nanoclusters in the O 1s (D) binding energy region: the blue and cyan Gaussians refer to the 532.0 and 533.1 eV components, respectively. For both C and D figures, the wine line refers to the background and the red line superimposed to the black experimental profile refers to the sum of the two Gaussian components.

due to the oxygen of the monoethanolamine capping layer that stabilises the Cu nanoclusters while the component at 533.1 eV is due to the oxygen of the Si/SiO_2 substrate.[46]

Magnetic and EPR characterization

EPR spectroscopy of both the pure oil and the water suspension of the synthesized material was measured at 40 K to evaluate the magnetic features of the sample, where Cu NCs are supposed to be diamagnetic. Both samples show a weak spectrum (Fig. 6), remarkably similar and characteristic of copper(II) in elongated coordination geometry, with $g_{\parallel} > g_{\perp} > g_e$ and $A_{\parallel} > A_{\perp}$ (where A_{ii} are the principal components of the hyperfine coupling tensor with the $I = 3/2$ nuclear spin of ^{63}Cu and ^{65}Cu). The similarity of the spectra in the two samples, with the clearly resolved parallel hyperfine structure, testifies that the paramagnetic centres are not clustered together and can be safely attributed to a paramagnetic impurity fraction of an otherwise diamagnetic sample. The best simulation of the spectra (reported in Fig. 6) provides spin Hamiltonian parameters ($g_x = 2.044 \pm 0.001$, $g_y = 2.056 \pm 0.001$, $g_z = 2.234 \pm 0.001$; $A_x = A_y = 50 \pm 10$ MHz, $A_z = 563 \pm 1$ MHz) which are consistent with previously reported ones for copper(II) ethanolamine complexes.[51,52]

To obtain a quantitative estimate of the amount of paramagnetic fraction, we measured the field-dependent magnetization at 5 K (Fig. 7). When rescaled to the atomic weight of copper (see the Experimental section), the measured values highlight that the magnetic contribution is indeed extremely weak, with a high field value much lower than that expected for

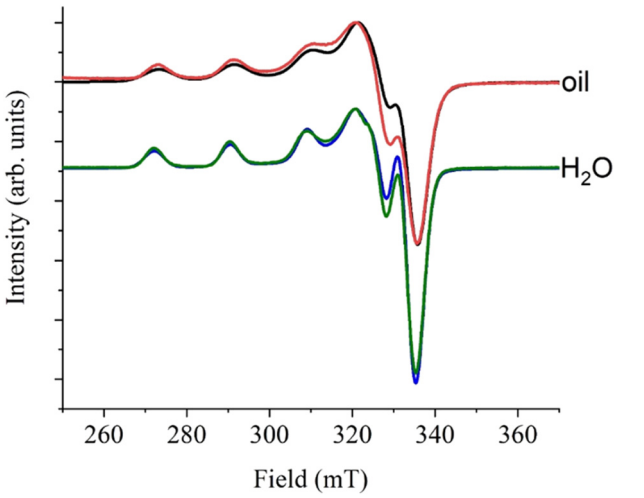

Fig. 6 X-band ($\nu \cong 9.40$ GHz) EPR spectra measured at 40 K for the oil (red trace) and water suspension (green trace) together with best simulations (black and blue lines) obtained using parameters reported in the text.

a pure $S = 1/2$ system. This is thus consistent with what is expected for metallic copper nanoclusters with a small impurity of a paramagnetic species Cu(II). The observed behaviour closely follows the expected one for a simple Brillouin system with a very low abundance of paramagnetic centres, which the fit (performed by fixing the g value to the average of the EPR determined ones, $g_{ave} = 2.111$) estimated to be $7.25 \pm 0.05\%$. In summary, the EPR and magnetic characterization unequivocally indicate the presence of a large majority of diamagnetic nanocluster with a small (<10%) amount of copper(II) complexes, in notable agreement with the results of the electrochemical characterization (*vide supra*).

Photothermal properties of Cu NCs

Although carbon and metal-based photothermal nanostructures have been investigated,[19,53–55] very few examples of photothermal

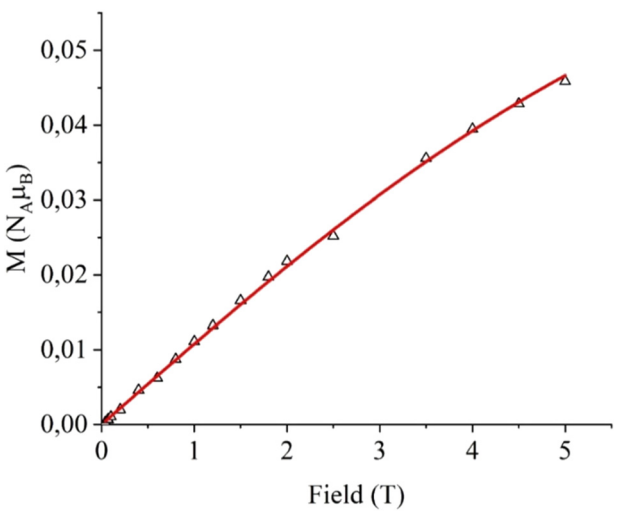

Fig. 7 Field-dependent magnetization of the oil sample measured at 5 K and best fit using Brillouin function with parameters reported in the text.

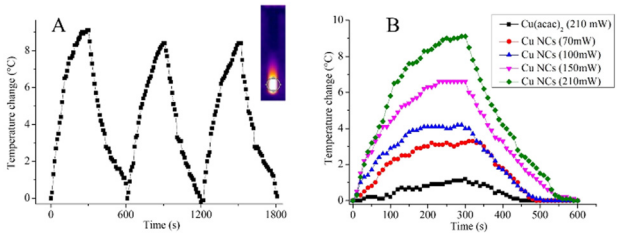

Fig. 8 Photothermal experiments for Cu NCs dispersion. (A) Photothermal heating–cooling cycles of the Cu NC nanostructure water dispersion, volume 100 μL, Abs_{405nm} = 0.36 in a glass tube (insets representative thermograph during photothermal experiments in a quartz tube) and (B) photothermal effect of the Cu NCs dispersion at different laser power.

Cu^0 nanomaterials are reported in the literature.[20–22] To investigate the photothermal properties of Cu NCs, an aqueous dispersion (100 mL, Abs_{405nm} = 0.36) was continuously exposed to a 405 nm laser (210 mW). The temperature changes were monitored using a thermal camera (Fig. 8A). When the temperature of the system reached the maximum value (temperature change = $T_{max} - T_{environment}$ = 9 °C), the laser was turned off, and the temperature change was monitored during the cooling process to confirm the heat transfer of the system. Three representative photothermal cycles are reported to confirm the excellent stability of the Cu NCs upon UV (405 nm) light exposition. The power-dependent photothermal behaviour was confirmed by experiments performed with different laser powers of 70, 100, 150 and 210 mW. The temperature difference values recorded were about 3.2 °C, 4.1 °C, 6.5 °C and 9.12 °C, respectively (Fig. 8B). In contrast, when a water dispersion of precursor $Cu(acac)_2$ was exposed to a laser power of 210 mW, only a negligible increase in temperature was observed (black line Fig. 8B), thus confirming the photothermal properties of Cu NCs. A photothermal conversion efficiency (η) value of about 38%, with a photothermal time constant (τ_s) values of about 110 s were calculated using an already reported procedure (Fig. S4, ESI†).[56] These data confirm the excellent conversion efficiency of Cu NCs compared to similar Cu-nanostructures reported in the literature. In fact, Korgel and coworkers reported for Cu nanocrystals, doped with selenide, a η value of about 27%.[57] Zhao *et al.* synthesized copper-based nanostructures which exhibited a photothermal conversion efficiency of 10.6% under laser irradiation.[58]

Conclusions

In line with the pursuit of sustainable and environmentally benign approaches to nanomaterial synthesis, we proposed a green photochemical approach to synthesize Cu NCs capped with monoethanolamine in water. These Cu NCs have been characterized by morphological, optical, electric, electronic, and magnetic measurements. Both XPS results and the observation of the anodic oxidation peak ($Cu^0 \rightarrow Cu^{2+}$ at −0.11 V) confirmed the Cu^0 oxidation state in the prepared material. EPR and magnetic characterization, in agreement with electrochemical data, evidenced the persistence of some residual paramagnetic Cu^{2+} ions. Since STEM-EDXS elemental mapping distribution highlighted that only oxygen of ethanolamine was observed, thus suggesting that no oxidation of the Cu NCs occurred, the presence of Cu^{2+} ions is due to the incomplete photochemical reduction of the starting $Cu(acac)_2$ precursor, possibly due to the formation of a small fraction of copper(II) ethanolamine complexes before the reduction was complete. On the other hand, the obtained ethanolamine-capped Cu NCs are stable for months. We also observed a strong blue emission (at 460–490 nm) due to LMCT and LMMCT charge transfers in self-assembled Cu NCs.

The reported results unequivocally demonstrate that Cu NCs are temporally and thermally stable for months and open the way to produce Cu NCs with adapted properties for potential technological uses.

Author contributions

The manuscript was written with the contribution of all authors.

Data availability

The data supporting this article have been included in the main text and as part of the ESI.†

Conflicts of interest

There are no conflicts to declare.

Acknowledgements

The authors thank the University of Catania for the financial support of the PIA.CE.RI. MAF-MOF project 2020–2022 and the B.R.I.T. laboratory of the University of Catania for the availability of the XPS facility. This work has also been partially funded by the European Union (NextGeneration EU) through the MUR-PNRR project SAMOTHRACE (ECS00000022). L. S. acknowledges the support of MUR through Dipartimenti di Eccellenza 2023-2027 (DICUS 2.0, CUP B97G22000740001) to the Department of Chemistry "Ugo Schiff" of the University of Florence.

References

1 S. Wei, A. Li, J.-C. Liu, Z. Li, W. Chen, Y. Gong, Q. Zhang, W.-C. Cheong, Y. Wang, L. Zheng, H. Xiao, C. Chen, D. Wang, Q. Peng, L. Gu, X. Han, J. Li and Y. Li, *Nat. Nanotechnol.*, 2018, **13**, 856–861.
2 X. Wang, J. Zhuang, Q. Peng and Y. Li, *Nature*, 2005, **437**, 121–124.
3 R. Jin, C. Zeng, M. Zhou and Y. Chen, *Chem. Rev.*, 2016, **116**, 10346–10413.
4 Y. Du, H. Sheng, D. Astruc and M. Zhu, *Chem. Rev.*, 2020, **120**, 526–622.
5 L. Zhang and E. Wang, *Nano Today*, 2014, **9**, 132–157.

6 M. G. Taylor and G. Mpourmpakis, *Nat. Commun.*, 2017, **8**, 15988.
7 X. Kang and M. Zhu, *Chem. Soc. Rev.*, 2019, **48**, 2422–2457.
8 Y. An, Y. Ren, M. Bick, A. Dudek, E. H.-W. Waworuntu, J. Tang, J. Chen and B. Chang, *Biosens. Bioelectron.*, 2020, **154**, 112078.
9 X. Liu and D. Astruc, *Coord. Chem. Rev.*, 2018, **359**, 112–126.
10 L. A. Peyser, A. E. Vinson, A. P. Bartko and R. M. Dickson, *Science*, 2001, **291**, 103–106.
11 C. Vázquez-Vázquez, M. Banobre-Lopez, A. Mitra, M. A. Lopez-Quintela and J. Rivas, *Langmuir*, 2009, **25**, 8208–8216.
12 Y. Chen, T. Yang, H. Pan, Y. Yuan, L. Chen, M. Liu, K. Zhang, S. Zhang, P. Wu and J. Xu, *J. Am. Chem. Soc.*, 2014, **136**, 1686–1689.
13 Z. Luo, X. Yuan, Y. Yu, Q. Zhang, D. T. Leong, J. Y. Lee and J. Xie, *J. Am. Chem. Soc.*, 2012, **134**, 16662–16670.
14 A. Baghdasaryan and T. Bürgi, *Nanoscale*, 2021, **13**, 6283–6340.
15 S. Giuffrida, G. G. Condorelli, L. L. Costanzo, I. L. Fragalà, G. Ventimiglia and G. Vecchio, *Chem. Mater.*, 2004, **16**, 1260–1266.
16 G. G. Condorelli, L. L. Costanzo, I. L. Fragalà, S. Giuffrida and G. Ventimiglia, *J. Mater. Chem.*, 2003, **13**, 2409–2411.
17 X. Zhu, B. Wang, F. Shi and J. Nie, *Langmuir*, 2012, **28**, 14461–14469.
18 R. Gui, J. Sun, X. Cao, Y. Wang and H. Jin, *RSC Adv.*, 2014, **4**, 29083–29088.
19 G. M. Consoli, G. Forte, L. Maugeri, V. Consoli, V. Sorrenti, L. Vanella, G. Buscarino, S. Agnello, M. Camarda, G. Granata, L. Ferreri and S. Petralia, *ACS Appl. Nano Mater.*, 2022, **6**, 358–369.
20 P. Huang, L. Kong, F. Zhang, L. Chen, Y. Zhang, X. Shi, T. Lawson, S. Chou, Y. Liu and W. Wu, *Small*, 2024, 2312211.
21 J. Wang, Y. Gu, Y. Fan and M. Yang, *ACS Appl. Nano Mater.*, 2023, **6**, 13561–13569.
22 J. Zhang, P. Li, T. Wang, J. Li, K. Yun, X. Zhang and X. Yang, *Pharmacol. Res.*, 2023, **187**, 106632.
23 A. Zhao, Z. Li and H. Wang, *Polymer*, 2010, **51**, 2099–2105.
24 C. I. Olariu, H. H. P. Yiu, L. Bouffier, T. Nedjadi, E. Costello, S. R. Williams, C. M. Halloran and M. J. Rosseinsky, *J. Mater. Chem.*, 2011, **21**, 12650–12659.
25 A. Gulino, *Anal. Bioanal. Chem.*, 2013, **405**, 1479–1495.
26 D. Briggs and J. T. Grant, *Surface analysis by Auger and X-ray photoelectron spectroscopy*, Chichester, UK, 2003.
27 G. Greczynski and L. Hultman, *Angew. Chem.*, 2020, **59**, 5002–5006.
28 S. Sharma, S. Das, K. Kaushik, A. Yadav, A. Patra and C. K. Nandi, *J. Phys. Chem. Lett.*, 2023, **14**, 8979–8987.
29 A. Ferlazzo, C. Espro, D. Iannazzo and G. Neri, *IEEE Trans. Instrum. Meas.*, 2023, **72**, 9508308.
30 S. Stoll and A. Schweiger, *J. Magn. Reson.*, 2006, **178**, 42–55.
31 Z. Wang, B. Chen, A. S. Susha, W. Wang, C. J. Reckmeier, R. Chen, H. Zhong and A. Rogach, *Adv. Sci.*, 2016, **3**, 1600182.
32 A. Baghdasaryan, R. Grillo, S. Roy Bhattacharya, M. Sharma, E. Reginato, H. Theraulaz, I. Dolamic, M. Dadras, S. Rudaz, E. Varesio and T. Burgi, *ACS Appl. Nano Mater.*, 2018, **1**, 4258–4267.
33 Q. Sun, Z. Ning, E. Yang, F. Yin, G. Wu, Y. Zhang and Y. Shen, *Angew. Chem.*, 2023, **135**, e202312.
34 A. Dutta, U. Goswami and A. Chattopadhyay, *ACS Appl. Mater. Interfaces*, 2018, **10**, 19459–19472.
35 Z. Wu, J. Liu, Y. Gao, H. Liu, T. Li, H. Zou, Z. Wang, K. Zhang, Y. Wang, H. Zhang and B. Yang, *J. Am. Chem. Soc.*, 2015, **137**, 12906–12913.
36 Y. Chen, T. Yang, H. Pan, Y. Yuan, L. Chen, M. Liu, K. Zhang, S. Zhang, P. Wu and J. Xu, *J. Am. Chem. Soc.*, 2014, **136**, 1686–1689.
37 Q. Benito, X. F. Le Goff, S. Maron, A. Fargues, A. Garcia, C. Martineau, F. Taulelle, S. Kahlal, T. Gacoin, J. P. Boilot and S. Perruchas, *J. Am. Chem. Soc.*, 2014, **136**, 11311–11320.
38 Z. Luo, X. Yuan, Y. Yu, Q. Zhang, D. T. Leong, J. Y. Lee and J. Xie, *J. Am. Chem. Soc.*, 2012, **134**, 16662–16670.
39 J. Mei, Y. Hong, J. W. Y. Lam, A. Qin, Y. Tang and B. Z. Tang, *Adv. Mater.*, 2014, **26**, 5429–5479.
40 P. Duan, N. Yanai, Y. Kurashige and N. Kimizuka, *Angew. Chem.*, 2015, **54**, 7544–7549.
41 Y. Yuan, C. J. Zhang, M. Gao, R. Zhang, B. Z. Tang and B. Liu, *Angew. Chem.*, 2015, **54**, 1780–1786.
42 S. Giuffrida, L. L. Costanzo, G. Ventimiglia and C. Bongiorno, *J. Nanopart. Res.*, 2008, **10**, 1183–1192.
43 A. Ferlazzo, C. Espro, D. Iannazzo, A. Bonavita and G. Neri, *Mater. Today Commun.*, 2023, **35**, 106036.
44 K. Ngamchuea, S. Wannapaiboon, P. Nongkhunsan, P. Hirunsit and I. Fongkaew, *J. Electrochem. Soc.*, 2022, **169**, 020567.
45 S. Li, H. Zhang, Z. Liu, J. Xu, G. Fan, W. Li, Q. Li, X. Hu and G. Jing, *Appl. Sci.*, 2022, **12**, 1245.
46 A. Gulino, G. G. Condorelli, P. Mineo and I. Fragalà, *Nanotechnology*, 2005, **16**, 2170–2175.
47 M. P. Seah, I. S. Gilmore and G. Beamson, *Surf. Interface Anal.*, 1998, **26**, 642–649.
48 Y. Zhang, J. Zhang, Z. Li, Z. Qin, S. Sharma and G. Li, *Commun. Chem.*, 2023, **6**, 24.
49 H. Keisar, G. de Ruiter, A. H. Velders, P. Milko, A. Gulino, G. Evmenenko, L. J. W. Shimon, Y. Diskin-Posner, M. Lahav and M. E. van der Boom, *J. Am. Chem. Soc.*, 2018, **140**, 8162–8171.
50 A. Gulino, S. Bazzano, P. Mineo, E. Scamporrino, D. Vitalini and I. Fragalà, *Chem. Mater.*, 2005, **17**, 521–526.
51 R. Tauler, E. Casassas and B. M. Rode, *Inorg. Chim. Acta*, 1986, **114**, 203–209.
52 S. K. Hoffmann, J. Goslar, I. Polus and B. Mazela, *Appl. Magn. Reson.*, 2003, **24**, 321–331.
53 G. M. L. Consoli, L. Maugeri, G. Forte, G. Buscarino, A. Gulino, L. Lanzanò, P. Bonacci, N. Musso and S. Petralia, *J. Mater. Chem. B*, 2024, **12**, 952–961.
54 G. M. L. Consoli, M. L. Giuffrida, S. Zimbone, L. Ferreri, L. Maugeri, M. Palmieri, C. Satriano, G. Forte and S. Petralia, *ACS Appl. Mater. Interfaces*, 2023, **15**, 5732–5743.
55 G. M. L. Consoli, M. L. Giuffrida, C. Satriano, T. Musumeci, G. Forte and S. Petralia, *Chem. Commun.*, 2022, **58**, 3126–3129.
56 G. M. L. Consoli, L. Maugeri, N. Musso, A. Gulino, L. D'Urso, P. Bonacci, G. Buscarino, G. Forte and S. Petralia, *Adv. Healthcare Mater.*, 2024, 2303692.
57 C. M. Hessel, V. P. Pattani, M. Rasch, M. G. Panthani, B. Koo, J. W. Tunnell and B. A. Korgel, *Nano Lett.*, 2011, **11**(6), 2560–2566.
58 H. Xiang, F. Xue, T. Yi, H. P. Tham, J.-G. Liu and Y. Zhao, *ACS Appl. Mater. Interfaces*, 2018, **10**, 16344–16351.